



Hydrate adhesive and tensile strengths

J. W. Jung and J. Carlos Santamarina

School of Civil and Environmental Engineering, Georgia Institute of Technology, 710 Atlantic Drive, NW, Atlanta, Georgia 30332, USA (kocee76@hotmail.com)

[1] The physical properties of hydrate-bearing sediments depend on the interaction between hydrates and minerals. In particular, hydrates prefer to nucleate on mineral surfaces, therefore, the hydrate-mineral adhesive strength and the tensile strength of the hydrate mass itself affect the mechanical response of hydrate-bearing sediments. In this study, ice and hydrates made with various guest molecules (CO₂, CH₄, and THF) are formed between mica and calcite substrates. Adhesive and tensile strengths are measured by applying an external pull-out force. Results show that tensile failure occurs in CO₂ and CH₄ hydrates when calcite is the substrate, while ice and all hydrates exhibit adhesive failure on mica. The debonding strength is higher when calcite substrates are involved rather than mica substrates. A nominal pull-out strength of 0.15 ± 0.03 MPa can be adopted for mechanical analyses of hydrate-bearing sediments.

Components: 6700 words, 6 figures, 1 table.

Keywords: adhesive; bonding; hydrate; strength; tensile.

Index Terms: 3004 Marine Geology and Geophysics: Gas and hydrate systems.

Received 3 January 2011; **Revised** 5 May 2011; **Accepted** 13 May 2011; **Published** 10 August 2011.

Jung, J. W., and J. C. Santamarina (2011), Hydrate adhesive and tensile strengths, *Geochem. Geophys. Geosyst.*, 12, Q08003, doi:10.1029/2010GC003495.

1. Introduction

[2] Gas hydrates consist of guest gas molecules encaged in water molecules. The most common gas molecule is methane, an abundant potential source of energy, with worldwide reserves on the order of 500 to 10,000 Gt of carbon [Collett, 2002; Kvenvolden, 1988; Ruppel and Pohlman, 2008]. Geomechanical analyses of hydrate-bearing sediments are necessary to assess the evolution of the formation during or after gas production, or during natural processes that may cause dissociation in hydrate-bearing sediments [Nixon and Grozic, 2007; Rutqvist and Moridis, 2007; Rutqvist et al., 2009].

[3] The mechanical and conduction properties of hydrate-bearing sediments are affected by the hydrate pore habit and the bonding characteristics between hydrate and mineral (general review by

Waite et al. [2009]). Similarly, hydrate growth or bonding onto pipe surfaces can have important effects on fluid flow. Hydrates prefer to nucleate on mineral surface if favored on mineral surfaces [Fletcher, 1969; Kashchiev and Firoozabadi, 2002]. Molecular dynamic simulations corroborate experimental observations and thermodynamic predictions and show lower activity near substrates and early water structuring that favors nucleation [Kvamme et al., 2007; see also Clennell et al., 1999].

[4] Once in contact with the mineral or metal surface, the hydrate tensile strength or the hydrate-substrate adhesive strength affect the strength and volume change behavior of hydrate-bearing sediments subjected to shear and the shear resistance to fluid drag in pipes (see Brugada et al. [2010] and J. W. Jung, J. C. Santamarina, and K. Soga (Stress-strain response of hydrate-bearing sediments, numerical study using DEM



Table 1. Ice and Hydrate Strengths: Compilation of Published Results

Material	Strength Mode	Strength (MPa)	Conditions	References
Ice	Tensile strength	0.7 to 3.1	T = 253–273 K, Strain rate = 10^{-8} – 10^{-3} s ⁻¹	Petrovic [2003]
		0.8 to 1.3	T = 263 K, Strain rate = 10^{-6} s ⁻¹	Currier and Schulson [1982]
	Compressive strength	5 to 35	T = 253–273 K, Strain rate = 10^{-8} – 10^{-3} s ⁻¹	Petrovic [2003]
Ice-substrate	Adhesive shear strength	0.21 to 0.34	Aluminum substrate, T = 263 K	Javan-Mashmool et al. [2006]
		0.53 to 0.54	Stainless steel substrate, T = 263 K	Jellinek [1959]
		0.19 to 3.3	Polystyrene substrate, T = 263 K	Jellinek [1959]
Methane hydrate	Compressive strength	0.015 to 0.084	Between ice substrates in air, T = 267–270 K	Fan et al. [2003]
		0.001 to 0.002 ^a	Between ice substrate in air, T = 263–271 K	Yang et al. [2004]
		2 to 10	T = 243–263 K, Confining pressure: 2–6 MPa Strain rate = 6–120 s ⁻¹	Nabeshima and Takai [2005]
		55.7 to 101.7	T = 260–287 K, P = 10–15 MPa Confining pressure: 50 MPa Strain rate = 10^{-8} – 10^{-5} s ⁻¹	Durham et al. [2003b]
		62 to 102	T = 140–260 K, Strain rate = 10^{-6} – 10^{-4} s ⁻¹	Stern et al. [1996, 1998, 2000]
		2 to 10	Confining pressure: 50–100 MPa T = 243–278 K, Confining pressure: 0–8 MPa Strain rate = 6–60 s ⁻¹	Hyodo et al. [2002]
THF hydrate + substrate	Adhesive strength	0.0006 to 0.0025 ^a	T = 261–275 K, Atmospheric pressure, THF hydrate	Taylor et al. [2007]
		0.0007 to 0.0014 ^a	Between THF substrates T = 263–271 K	Yang et al. [2004]

^aEstimated from the published results.

simulations, submitted to *Journal of Geophysical Research*, 2011) for discrete element simulation results). However, most of the available strength data correspond to compressive loading. The purpose of this study is to determine the adhesive and tensile strengths of CH₄ hydrate, CO₂ hydrate, tetrahydrofuran THF hydrate, and ice to calcite and mica substrates (Table 1).

2. Previous Studies

[5] Water and mineral interaction before hydrate formation are determined by surface charge. Mica (Muscovite-K₂O·Al₂O₃·SiO₂) has a negative surface charge at its equilibrium pH, forms a strong hydrogen bond with water, and exhibits a low contact angle ($\theta < \sim 5^\circ$) [Maslova et al., 2004]. On the other hand, calcite (CaCO₃) has a positive surface charge, forms a weak bond with water and the water-vapor-calcite contact angle is high ($\theta = \sim 37^\circ$) [Osawa et al., 2008].

[6] After phase transformation, ice or hydrate can mobilize additional mechanical interaction effects with the mineral. For example, an increase in surface roughness typically results in greater adhesive strength due to the increase in the total effective area available for adhesion and the development of mechanical interlocking ([Adamson, 1997; Petrie, 2007] note that roughness may decrease strength if it prevents the formation of contacts when a hydrate mass is brought into contact with the substrate). We note that a thin liquid-like layer may remain between ice or hydrate and the mineral surface; then, capillary adhesion may dominate the adhesive strength between hydrate and atomically smooth mineral surfaces [Anklam et al., 2008; Churaev, 2004; Clennell et al., 1999; Fan et al., 2003; Tsionsky et al., 2005].

[7] Previous studies on the strength of ice and hydrate emphasized compressive strength. The compressive strength of ice is inversely proportional to temperature and it can range from 5 MPa at 0°C to 25 MPa at -20°C [Petrovic, 2003]. The tensile strength of ice is less sensitive to temperature and varies from 0.7 MPa at 0°C to 3.1 MPa at -20°C [Petrovic, 2003]. The ratio between the tensile σ_t and compressive σ_c strengths for ice varies with temperature T [°C] as follows [Petrovic, 2003]:

$$\sigma_c/\sigma_t = -0.1789 \cdot T + 3.9653 \text{ between } 0^\circ\text{C and } -35^\circ\text{C.} \quad (1)$$

Both tensile and compressive strengths are proportional to strain rate, and inversely proportional to

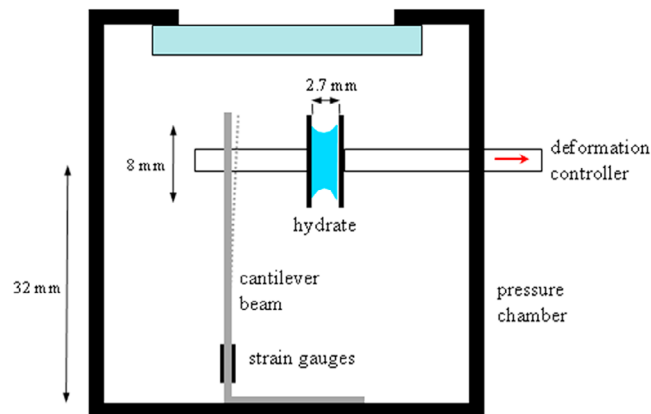


Figure 1. Device built to measure tensile strength. The load cell consists of a cantilever beam instrumented with strain gauges. The device is placed inside P-T controlled pressure chamber (Sketch is not to scale; dimensions are in millimeters).

specimen size and grain size [Petrovic, 2003]. The ice-substrate adhesive strength depends on the substrate material and temperature. For reference, consider the following reported values: $\sigma_t = 0.21$ to 0.34 MPa for ice-aluminum at [Javan-Mashmool *et al.*, 2006], $\sigma_t = 0.19$ to 0.33 MPa for ice-polystyrene at -5°C , and $\sigma_t = 0.53$ to 0.54 MPa for ice-stainless steel at -10°C [Jellinek, 1959].

[8] The compressive strength of methane hydrate can be 20 times higher than that of ice [Durham *et al.*, 2003b]. The compressive strength of methane hydrate is inversely proportional to temperature and directly proportional to strain rate and confining pressure [Durham *et al.*, 2003a, 2003b; Hyodo *et al.*, 2002; Nabeshima and Takai, 2005; Stern *et al.*, 1996, 1998, 2000]. The adhesive strength between two THF hydrate particles increases with the contact duration t^* and the ambient temperature, for example, from 0.45 to 1.78 kPa when the contact duration increases from 1 s to 40000 s, and from 0.63 to 2.55 kPa when the temperature increases from $+2.5^\circ\text{C}$ to -10°C (subcooling dependent) [Nicholas *et al.*, 2009; Taylor *et al.*, 2007; Yang *et al.*, 2004].

3. Experimental Study

3.1. Equipment and Materials

3.1.1. Device for Tensile Stress Measurements

[9] Two substrates of the same mineral were positioned parallel to each other to form a cylindrical body of either ice or hydrate between them (Figure 1). One substrate was mounted on a deformation-controlled driver that was used to impose the horizontal pull-out motion (Figure 1). The other

substrate rested on a relatively rigid cantilever beam that was instrumented with strain gauges to measure the pull-out force (General Multi Purpose Linear Pattern Strain gage from Vishay). The full bridge circuit had two active gauges and two dummy gauges for temperature compensation. The cantilever beam load cell was calibrated using gravity loading.

3.1.2. Pressure Chamber

[10] The device was placed inside a high-pressure chamber that has a sapphire window to observe the evolution of the test. The chamber was surrounded by a copper pipe and an insulation layer to control temperature. Cell pressure and temperature were continuously recorded using a data logger.

3.1.3. Materials

[11] Two mineral substrates were used in this study: mica (Muscovite- $\text{K}_2\text{O}\cdot\text{Al}_2\text{O}_3\cdot\text{SiO}_2$) and a calcite crystal (CaCO_3). The mineral substrates were cemented using cyanoacrylate onto the steel pedestals mounted on the cantilever beam and the deformation-controlled driver. The guest molecules selected for hydrate formation were CH_4 , CO_2 , and THF. The THF solution is 81% H_2O and 19% THF by mass to form 100% hydrate (i.e., stoichiometric mixture $\text{THF}\cdot 17\text{H}_2\text{O}$). An additional series of tests was conducted on ice.

3.2. Test Procedure

3.2.1. Specimen Preparation

[12] The instrumented cantilever beam, the deformation controller and the chamber were assembled

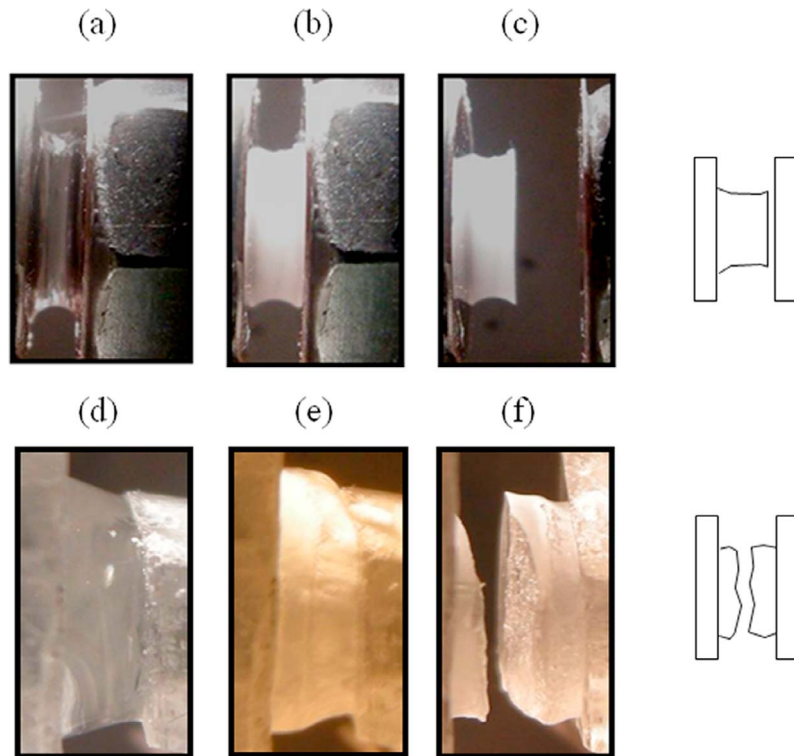


Figure 2. Experimental results: (a) water meniscus between mica substrates, (b) CH₄ hydrate formation, (c) adhesive failure between CH₄ hydrate and mica substrate, (d) water meniscus between calcite substrates, (e) CH₄ hydrate formation, and (f) tensile failure between CH₄ hydrate and calcite substrate.

together. A 2.7 mm gap was left between the two parallel substrates. Then, a droplet of water was placed between the substrates to form a quasi-cylindrical specimen (height = 2.7 mm, diameter = 4.8 to 8.6 mm, mass = 63 to 202 mg; note that while the water droplet was stable when the mica substrates were vertically aligned, tests with calcite substrates required turning the chamber to align the substrates in the horizontal direction so that the water meniscus would remain in place). Finally, the chamber was closed and ready for testing.

3.2.2. Ice and Hydrate Formation

[13] Ice was formed at atmospheric pressure and tests were conducted at a temperature of -5°C . The THF solution forms hydrate structure II under an atmospheric pressure of $\sim 4.4^{\circ}\text{C}$; the THF hydrate was tested at a temperature slightly above $\sim 0^{\circ}\text{C}$ to avoid any ice formation. The two gas hydrates were formed by filling the chamber with gas, followed by pressurization (~ 8 MPa for CH₄ hydrate, and ~ 3.5 MPa for CO₂ hydrate) while lowering the temperature to $\sim 2^{\circ}\text{C}$ (the phase boundaries at 2°C are at 2.8 MPa for CH₄ hydrate and at 1.5 MPa for CO₂ hydrate). Hydrate formation was confirmed by

visual inspection through the sapphire window (Figures 2b and 2e) and by the exothermic response detected with the thermocouple.

3.2.3. Tensile Load

[14] The induction time for hydrate formation ranged from 8 to 17 h; for comparison, the diffusion time for CO₂ and CH₄ in water is around $t = (d/2)^2/D = 1.6$ to 5.1 h (where d = meniscus diameter, D = diffusivity; data in the study by Jung *et al.* [2010]). The pull-out tests were run about ~ 10 h after hydrate or ice formation. The bridge output was recorded every 2 ms and converted to force using the calibrated response. The pull-out force was increased until failure (Figure 3). Tensile or debonding failure were determined from microphotographs obtained through the sapphire window immediately after the failure (examples in Figure 2c).

4. Experimental Results

4.1. Failure Mode

[15] Debonding failure occurred in all cases when mica was the substrate, including ice and all hydrates

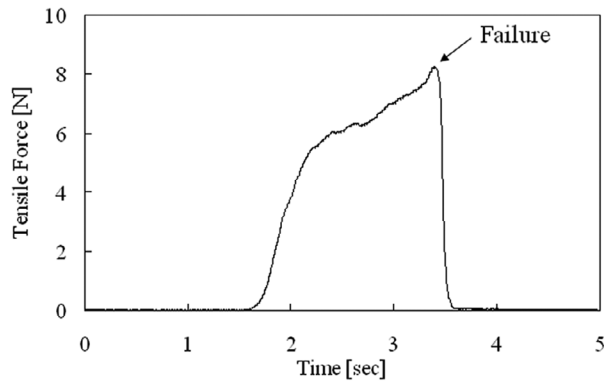


Figure 3. Typical force-time response (case: CH₄ hydrate on a calcite substrate).

(e.g., CH₄ hydrate, CO₂ hydrate, THF hydrate). When calcite was involved, the failure mode was tensile failure for CH₄ and CO₂ hydrates and debonding failure for THF hydrate and ice (see summary in Figure 4; note that upper and lower bound strength estimates for CH₄ and CO₂ hydrates are discussed in the next section). Differences in failure mode could relate (1) to the role of impurities on mineral surfaces and their effect on nucleation and crystal growth, and (2) to differences in electrical interactions, such as marked water-mineral affinity that could hinder hydrate formation on the mineral surface [Kvamme et al., 2007]. Mica has oxygen on the surface and evolves stronger H bond interaction with water than calcite which has cal-

cium ions on the surface [Perry et al., 2007; Wang et al., 2009, 2005].

4.2. Strength

[16] Both the THF solution and water convert into a 100% solid mass of either THF hydrate or ice. In these two cases, the pull-out force is divided by the specimen cross-sectional area to compute strength. The computation of strength is more complex in the case of diffusion- and solubility-limited CO₂ and CH₄ hydrate formation. The lower bound strength is estimated assuming that the complete water mass converted into hydrate. The upper bound requires estimating the thickness of the hydrate ring that forms when hydrate grows from the liquid-gas interface into the liquid phase (J. W. Jung and J. C. Santamarina, Hydrate formation and growth in pores, submitted to *Journal of Crystal Growth*, 2011): experimental results suggest that the hydrate thickness 10 h after initial formation can reach 1.9 to 2.3 mm when hydrophilic substrates are used and 2.1 to 2.3 mm on hydrophobic substrates; using this estimate of thickness, we compute an upper bound for the tensile strength of CH₄ and CO₂ hydrates. Results in Figure 4 show (1) that the adhesive strength is higher when calcite is involved (this applies to all cases, including CO₂ and CH₄ hydrates which failed in tension before debonding) and (2) that the pull-out strength limited by either tensile or adhesive failure will rarely exceed 0.20 MPa.

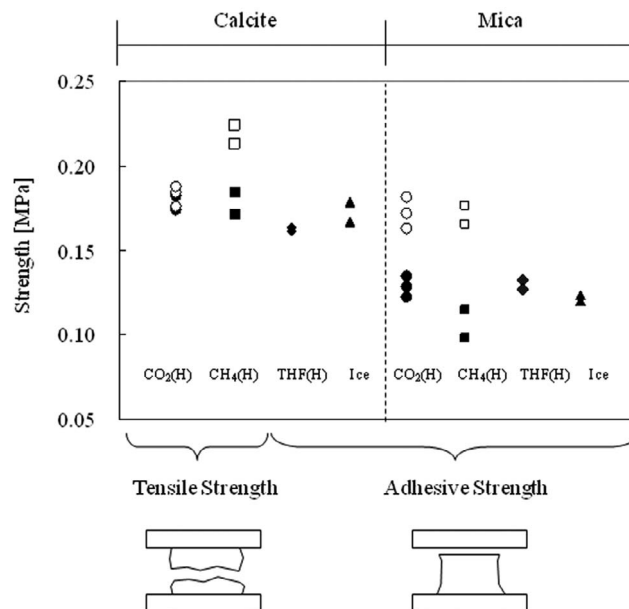


Figure 4. Hydrate adhesive and tensile strengths. Assumed cross section: filled symbols correspond to 100% formation, while empty symbols correspond to annular hydrate formation. (Refer to Table 1 for previous studies.)

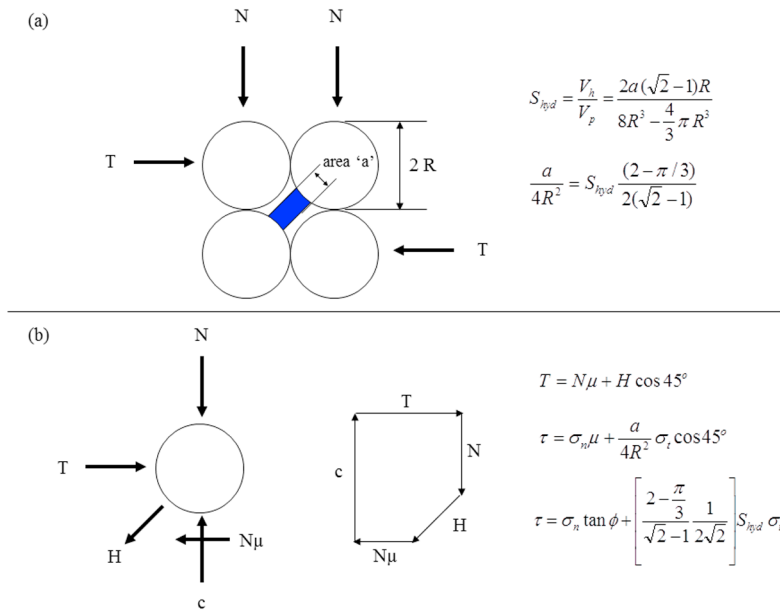


Figure 5. The relevance of tensile or adhesive hydrate strength on the shear strength of hydrate-bearing sediments. (a) Bonded hydrate mass in a simple cubic packing configuration. (b) Force diagram for a single particle.

[17] Calcite surfaces used in this study were rougher than the atomically smooth freshly peeled mica surface [see also *Szozkiewicz et al.*, 2005]. Increased surface area available for bonding, and mechanical interlocking can contribute to the higher adhesive strengths exhibited by all hydrates and ice when calcite was involved.

5. Analyses and Discussion

5.1. Adhesive Strength

[18] Values measured in this study are 2 orders of magnitude greater than previously reported values of adhesive strength between hydrate-substrate or hydrate-hydrate surfaces brought into contact [*Aspenes et al.*, 2010; *Nicholas et al.*, 2009]. This result shows that hydrates that nucleate and grow on a solid surface experience significantly greater adhesive strength than when the hydrate mass contacts a solid surface after hydrate formation. Possible contributing factors include (1) the role of surface roughness allowing for hydrate growth in crevices, versus roughness reducing the number of contact points when solids are brought into contact and (2) the displacement of surface impurities during hydrate nucleation and growth, versus impurities preventing bonding when two solids approach each other. In addition, devices used to measure adhesive strength also affect the measured

values: flexible beams impose a “peel-off” type of mechanical action which is equivalent to a propagating local tensile failure (as in the study by *Aspenes et al.* [2010] and *Nicholas et al.* [2009]); in contrast, the more rigid pull-out system used in this study imposes a relatively homogeneous tension throughout the specimen.

5.2. Implication on the Shear Strength of Hydrate-Bearing Sediments

[19] Published experimental results show that the shear strength τ_f of hydrate-bearing sediments is a function of the normal stress σ_n , the friction angle ϕ , hydrate saturation S_h , and hydrate habit in pores [*Ebinuma et al.*, 2005; *Hyodo et al.*, 2008; *Masui et al.*, 2005; *Yun et al.*, 2007]. The simple cubic packing of round mineral grains size R sketched in Figure 5 helps assess the interplay between these parameters. The shear force T required to shear the upper row of particles relative to the lower row is related to the normal load N , the interparticle friction coefficient μ , the cross-sectional area of the hydrate mass a and the hydrate tensile/bonding strength σ_i (note that the compressive resistance of a transverse hydrate “truss” is not included in this analysis to emphasize the limiting effect of a tensile failure):

$$T = N \cdot \mu + a \cdot \sigma_i \cdot \cos 45^\circ. \quad (2)$$

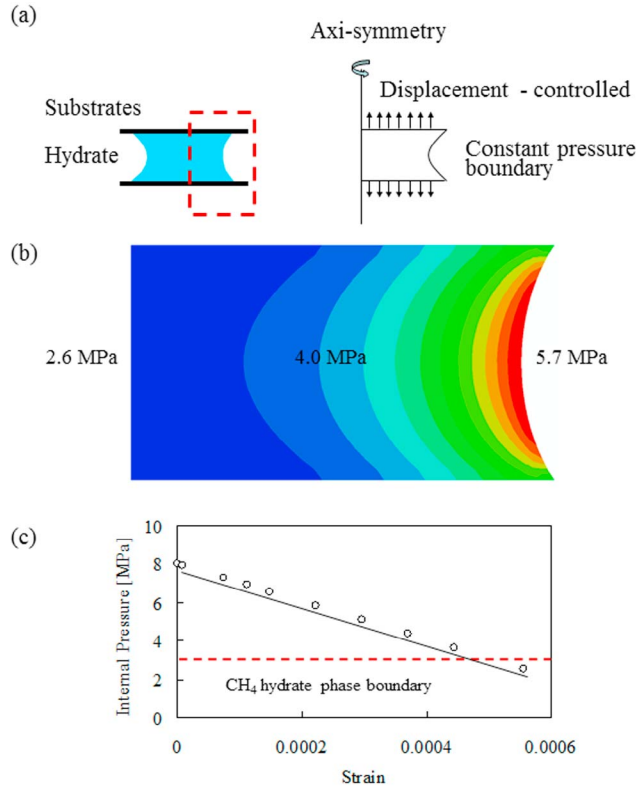


Figure 6. Internal pressure change during tensile loading. (a) Boundary conditions for FEM simulation. (b) Mean stress field (case: strain = 5.5×10^{-4} , $E = 8.2$ GPa, $\nu = 0.32$, $P = 8.0$ MPa). (c) Mean stress change during pull out as a function of longitudinal strain.

These parameters can be converted to distributed variables shear stress at failure τ_f , normal stress σ_n and hydrate saturation S_{hyd} using the following mechanical and geometric considerations (see details in Figure 5):

$$\tau_f = \frac{T}{4R^2}; \sigma_n = \frac{N}{4R^2}; S_{hyd} = \frac{V_h}{V_p} = \frac{2a(\sqrt{2}-1)R}{8R^3 - \frac{4}{3}\pi R^3}. \quad (3)$$

Then, equation (2) can be written in terms of distributed, equivalent continuum parameters as follows:

$$\tau_f = \sigma_n \tan \phi + 1.6 S_{hyd} \sigma_t. \quad (4)$$

This expression provides a first-order physical explanation to the effect of hydrate on the shear strength of hydrate-bearing sediments and shows that the hydrate-mineral tensile strength determines the Mohr-Coulomb cohesive intercept. Clearly, an alternative hydrate pore habit will have a different effect on strength.

5.3. Local Hydrate Dissociation

[20] We used finite elements to study the change in internal stress within the hydrate mass during tensile

loading. The simulation conducted in ABAQUS, involves an axisymmetric specimen geometry similar to the one observed in the experiments (Figure 6a). The hydrate mass is modeled as an isotropic linear-elastic body, bonded to the two end-platens, and subjected to a constant hydrostatic pressure at the hydrate-gas interface. The stress change within the specimen is monitored during the isothermal, displacement-controlled tensile test (Figure 6b). Results show that the mean stress at the center of the hydrate mass decreases and eventually migrates outside the hydrate stability field (Figure 6c). This suggests the possibility that the tensile failure of a hydrate mass may be the result of local stress conditions that cause hydrate dissociation.

6. Conclusions

[21] The hydrate-mineral adhesive strength and the tensile strength of the hydrate mass itself affect the mechanical response of hydrate-bearing sediments. Both tensile and debonding failures are dependent on mineral substrates. When mica is the substrate, debonding failure occurs for ice and all hydrates



(e.g., CH₄ hydrate, CO₂ hydrate, THF hydrate). When calcite is involved, the failure mode is tensile failure for CH₄ and CO₂ hydrates and debonding failure for THF hydrate and ice. Therefore, the adhesive strength is higher when calcite is involved in all cases, in part because calcite surfaces are rougher than atomically smooth freshly peeled mica surfaces. In addition, there is a lower probability of free water at the calcite-hydrate interface.

[22] The tensile strength of CH₄ and CO₂ hydrate is 0.20 ± 0.03 MPa. This strength is significantly greater than published adhesive strength values between a hydrate mass brought into contact with solid surface. It is anticipated that surface roughness and impurities play very different roles when hydrate nucleates onto the substrate and when the hydrate mass is brought into contact with the substrate.

[23] Soft-flexible devices may impose a “peel-off” type of loading which causes a propagating local tensile failure. In contrast, in-line pull-out systems create a homogeneous tension throughout the specimen and are prone to render a higher strength. Numerical FEM simulation results suggest the possibility that the tensile failure of the CO₂ and CH₄ hydrate mass may result from local hydrate dissociation during tensile loading due to an effective decrease in internal stress.

[24] The grain-scale adhesive and/or tensile strength between hydrate and mineral grains affects the strength of hydrate-bearing sediments. A particle-scale micromechanical model shows that the hydrate-mineral tensile strength determines the Mohr-Coulomb cohesive intercept.

Notation

θ	contact angle (°).
σ_t	tensile strength (MPa).
σ_c	compressive strength (MPa).
T	temperature (°C).
t	time (h).
d	meniscus diameter (m).
D	diffusivity (m ² /min).
τ_f	shear strength (MPa).
σ_n	normal stress (MPa).
ϕ	friction angle (°).
S_h	hydrate saturation.
R	radius mineral grain (m).
T	shear force (N).
N	normal force (N).

μ interparticle friction coefficient.

a cross-sectional area of the hydrate mass (m²).

Acknowledgments

[25] Support for this research was provided by the U.S. Department of Energy. Additional funding was provided by the Goizueta Foundation.

References

- Adamson, A. W. (1997), *Physical Chemistry of Surfaces*, 6th ed., John Wiley, New York.
- Anklam, M. R., J. D. York, L. Helmerich, and A. Firoozabadi (2008), Effects of antiagglomerants on the interactions between hydrate particles, *AICHE J.*, *54*(2), 565–574, doi:10.1002/aic.11378.
- Aspenes, G., L. E. Dieker, Z. M. Aman, S. Høiland, A. K. Sum, C. A. Koh, and E. D. Sloan (2010), Adhesion force between cyclopentane hydrates and solid surface materials, *J. Colloid Interface Sci.*, *343*(2), 529–536, doi:10.1016/j.jcis.2009.11.071.
- Brugada, J., Y. P. Cheng, K. Soga, and J. C. Santamarina (2010), Discrete element modelling of geomechanical behaviour of methane hydrate soils with pore-filling hydrate distribution, *Granul. Matter*, *12*(5), 517–525, doi:10.1007/s10035-010-0210-y.
- Churaev, N. V. (2004), Mass transfer in frozen porous bodies, *Colloid J.*, *66*(6), 751–755, doi:10.1007/s10595-005-0018-3.
- Clennell, B. M., M. Hovland, J. S. Booth, P. Henry, and W. J. Winters (1999), Formation of natural gas hydrates in marine sediments: 1. Conceptual model of gas hydrate growth conditioned by host sediment properties, *J. Geophys. Res.*, *104*(B10), 22,985–23,003, doi:10.1029/1999JB900175.
- Collett, T. S. (2002), Energy resource potential of natural gas hydrates, *AAPG Bull.*, *86*(11), 1971–1992.
- Currier, J. H., and E. M. Schulson (1982), The tensile-strength of ice as a function of grain-size, *Acta Metall. Mater.*, *30*(8), 1511–1514, doi:10.1016/0001-6160(82)90171-7.
- Durham, W. B., L. A. Stern, and S. H. Kirby (2003a), Ductile flow of methane hydrate, *Can. J. Phys.*, *81*, 373–380, doi:10.1139/p03-042.
- Durham, W. B., S. H. Kirby, L. A. Stern, and W. Zhang (2003b), The strength and rheology of methane clathrate hydrate, *J. Geophys. Res.*, *108*(B4), 2182, doi:10.1029/2002JB001872.
- Ebinuma, T., Y. Kamata, H. Minagawa, R. Ohmura, J. Nagao, and H. Narita (2005), Mechanical properties of sandy sediment containing methane hydrate, paper presented at Fifth International Conference on Gas Hydrate, Tapir Acad., Trondheim, Norway, 12–16 June.
- Fan, X., P. Ten, C. Clarke, A. Bramley, and Z. Zhang (2003), Direct measurement of the adhesive force between ice particles by micromanipulation, *Powder Technol.*, *131*(2–3), 105–110, doi:10.1016/S0032-5910(02)00339-X.
- Fletcher, N. H. (1969), Active sites and ice crystal nucleation, *J. Atmos. Sci.*, *26*(6), 1266–1271, doi:10.1175/1520-0469(1969)026<1266:ASAICN>2.0.CO;2.
- Hyodo, M., A. F. L. Hyde, Y. Nakata, N. Yoshimoto, M. Fukunaga, K. Kubo, Y. Nanjo, T. Matsuo, and K. Nakamura (2002), Triaxial compressive strength of methane hydrate, paper presented at 12th International Offshore



- and Polar Engineering Conference, Int. Soc. of Offshore and Polar Eng., Kitakyusu, Japan, 26–31 May.
- Hyodo, M., Y. Nakata, N. Yoshimoto, and J. Yoneda (2008), Shear strength of methane hydrate bearing sand and its deformation during dissociation of methane hydrate, paper presented at Fourth International Symposium on Deformation Characteristics of Geomaterials, Ga. Inst. of Technol., Atlanta, Ga.
- Javan-Mashmool, M., C. Volat, and M. Farzaneh (2006), A new method for measuring ice adhesion strength at an ice-substrate interface, *Hydrol. Processes*, *20*(4), 645–655, doi:10.1002/hyp.6110.
- Jellinek, H. H. G. (1959), Adhesive properties of ice, *J. Colloid Sci.*, *14*, 268–280, doi:10.1016/0095-8522(59)90051-0.
- Jung, J. W., D. N. Espinoza, and J. C. Santamarina (2010), Properties and phenomena relevant to CH₄-CO₂ replacement in hydrate-bearing sediments, *J. Geophys. Res.*, *115*, B10102, doi:10.1029/2009JB000812.
- Kashchiev, D., and A. Firoozabadi (2002), Nucleation of gas hydrates, *J. Cryst. Growth*, *243*(3–4), 476–489, doi:10.1016/S0022-0248(02)01576-2.
- Kvamme, B., A. Graue, T. Buanes, T. Kumetsoua, and G. Ersland (2007), Storage of CO₂ in natural gas hydrate reservoirs and the effect of hydrate as an extra sealing in cold aquifers, *Int. J. Greenhouse Gas Control*, *1*(2), 236–246, doi:10.1016/S1750-5836(06)00002-8.
- Kvenvolden, K. A. (1988), Methane hydrate—A major reservoir of carbon in the shallow geosphere, *Chem. Geol.*, *71*(1–3), 41–51, doi:10.1016/0009-2541(88)90104-0.
- Maslova, M. V., L. G. Gerasimova, and W. Forsling (2004), Surface properties of cleaved mica, *Colloid J.*, *66*(3), 322–328, doi:10.1023/B:COLL.0000030843.30563.c9.
- Masui, A., H. Haneda, Y. Ogata, and K. Aoki (2005), The effect of saturation degree of methane hydrates on the shear strength of synthetic methane hydrate sediments, paper presented at Fifth International Conference on Gas Hydrate, Trondheim, Norway, 12–16 June.
- Nabeshima, Y., and Y. Takai (2005), Compressive strength and density of methane hydrate, paper presented at Sixth Ocean Mining Symposium, Int. Soc. of Offshore and Polar Eng., Changsha, China, 9–13 Oct.
- Nicholas, J. W., L. E. Dieker, E. D. Sloan, and C. A. Koh (2009), Assessing the feasibility of hydrate deposition on pipeline walls—Adhesion force measurements of clathrate hydrate particles on carbon steel, *J. Colloid Interface Sci.*, *331*(2), 322–328, doi:10.1016/j.jcis.2008.11.070.
- Nixon, M. F., and J. L. H. Grozic (2007), Submarine slope failure due to gas hydrate dissociation: A preliminary quantification, *Can. Geotech. J.*, *44*(3), 314–325, doi:10.1139/t06-121.
- Osawa, M., M. Tsushima, H. Mogami, G. Samjeske, and A. Yamakata (2008), Structure of water at the electrified platinum water interface: A study by surface-enhanced infrared absorption spectroscopy, *J. Phys. Chem.*, *112*, 4248–4256.
- Perry, T. D., R. T. Cygan, and R. Mitchell (2007), Molecular models of a hydrated calcite mineral surface, *Geochim. Cosmochim. Acta*, *71*(24), 5876–5887, doi:10.1016/j.gca.2007.08.030.
- Petrie, E. M. (2007), *Handbook of Adhesives and Sealants*, 2nd ed., McGraw-Hill, New York.
- Petrovic, J. J. (2003), Mechanical properties of ice and snow, *J. Mater. Sci.*, *38*(1), 1–6, doi:10.1023/A:1021134128038.
- Ruppel, C., and J. W. Pohlman (2008), Climate change and the global carbon cycle: Perspectives and opportunities, *Fire in the Ice, Winter*, p. 5.
- Rutqvist, J., and G. J. Moridis (2007), Numerical studies of geomechanical stability of hydrate-bearing sediments, paper OTC 18860 presented at Offshore Technological Conference, Am. Assoc. of Pet. Geol., Houston, Tex., 30 April to 3 May.
- Rutqvist, J., G. J. Moridis, T. Grover, and T. Collett (2009), Geomechanical response of permafrost-associated hydrate deposits to depressurization-induced gas production, *J. Petrol. Sci. Eng.*, *67*(1–2), 1–12, doi:10.1016/j.petrol.2009.02.013.
- Stern, L. A., S. H. Kirby, and W. B. Durham (1996), Peculiarities of methane clathrate hydrate formation and solid-state deformation, including possible superheating of water ice, *Science*, *273*(5283), 1843–1848, doi:10.1126/science.273.5283.1843.
- Stern, L. A., S. H. Kirby, and W. B. Durham (1998), Polycrystalline methane hydrate: Synthesis from superheated ice, and low-temperature mechanical properties, *Energy Fuels*, *12*(2), 201–211, doi:10.1021/ef970167m.
- Stern, L. A., S. H. Kirby, W. B. Durham, S. Circone, and W. F. Waite (2000), *Natural Gas Hydrate in Oceanic and Permafrost Environments*, edited by M. D. Max, chap. 25, 323–348, Springer, New York.
- Szoszkiewicz, R., B. Bhushan, B. D. Huey, A. J. Kulik, and G. Gremaud (2005), Correlations between adhesion hysteresis and friction at molecular scales, *J. Chem. Phys.*, *122*, 144708, doi:10.1063/1.1886751.
- Taylor, C. J., L. E. Dieker, K. T. Miller, C. A. Koh, and E. D. Sloan (2007), Micromechanical adhesion force measurements between tetrahydrofuran hydrate particles, *J. Colloid Interface Sci.*, *306*(2), 255–261, doi:10.1016/j.jcis.2006.10.078.
- Tsionsky, V., E. Alengoz, L. Daikhin, A. Kaverin, D. Zagidulin, and E. Gileadi (2005), The liquid-like layer between metal and frozen aqueous electrolytes: An electrochemical approach employing the quartz crystal microbalance, *Electrochim. Acta*, *50*, 4212–4221, doi:10.1016/j.electacta.2005.02.088.
- Waite, W. F., et al. (2009), Physical properties of hydrate-bearing sediments, *Rev. Geophys.*, *47*, RG4003, doi:10.1029/2008RG000279.
- Wang, J., A. G. Kalinichev, R. J. Kirkpatrick, and R. T. Cygan (2005), Structure, energetics, and dynamics of water adsorbed on the muscovite (001) surface: A molecular dynamics simulation, *J. Phys. Chem.*, *109*, 15,893–15,905, doi:10.1021/jp045299c.
- Wang, J., A. G. Kalinichev, and R. J. Kirkpatrick (2009), Asymmetric hydrogen bonding and orientational ordering of water at hydrophobic and hydrophilic surfaces: A comparison of water/vapor, water/talc, and water/mica interface, *J. Phys. Chem. C*, *113*(25), 11,077–11,085, doi:10.1021/jp9018316.
- Yang, S. O., D. M. Kleehammer, Z. X. Huo, E. D. Sloan, and K. T. Miller (2004), Temperature dependence of particle-particle adherence forces in ice and clathrate hydrates, *J. Colloid Interface Sci.*, *277*(2), 335–341, doi:10.1016/j.jcis.2004.04.049.
- Yun, T. S., J. C. Santamarina, and C. Ruppel (2007), Mechanical properties of sand, silt, and clay containing tetrahydrofuran hydrate, *J. Geophys. Res.*, *112*, B04106, doi:10.1029/2006JB004484.